

We are IntechOpen, the world's leading publisher of Open Access books Built by scientists, for scientists

6,900

Open access books available

186,000

International authors and editors

200M

Downloads

Our authors are among the

154

Countries delivered to

TOP 1%

most cited scientists

12.2%

Contributors from top 500 universities



WEB OF SCIENCE™

Selection of our books indexed in the Book Citation Index
in Web of Science™ Core Collection (BKCI)

Interested in publishing with us?
Contact book.department@intechopen.com

Numbers displayed above are based on latest data collected.
For more information visit www.intechopen.com



Constitutive Modeling of Masonry Walls Strengthened with Fiber Reinforced Polymers

Bilge Doran, Hasan Orhun Köksal, Selen Aktan,
Oktay Jafarov and Cengiz Karakoç

Additional information is available at the end of the chapter

<http://dx.doi.org/10.5772/intechopen.77201>

Abstract

This study primarily focuses on the constitutive modeling of masonry walls strengthened with fiber-reinforced polymers (FRP). In general, providing suitable relations for the material characterization of the masonry constituents so that the nonlinear finite element (NLFEA) applications of the elasto-plastic theory achieves a close fit to the experimental load-displacement diagrams of the walls subjected to in-plane loadings is desired. In this chapter, two relations proposed for masonry columns confined with FRP are adjusted for the cohesion and the internal friction angle of both units and mortar. Relating the mechanical parameters to the uniaxial compression strength and the hydrostatic pressure acting over the wall surface, the effects of major and intermediate principal stresses σ_1 and σ_2 on the yielding and the shape of the deviatoric section are then reflected into the analyses. Finally, NLFEA results for the walls tested in different studies showed a good match with the experimental ones.

Keywords: masonry wall, fiber reinforced polymer, cohesion, internal friction, elasto-plastic analysis, finite element analysis

1. Introduction

Many historical masonry buildings of the world's architectural heritage are in dire need of retrofitting as they do not perform well to the seismic activities. Retrofitting of such structures needed better understanding of the constitutive features to characterize its present condition and determine the true structural safety for seismic actions. Although masonry has been used in building for centuries in many countries such as Turkey, constitutive

models and calculation techniques have not yet been available that allow realistic descriptions of the mechanic behavior of structures made of this heterogeneous material. During the last decade, the interest in seismic retrofitting of masonry structures has led to the development of specific engineering techniques and strategies in seismic areas. In this context, fiber-reinforced polymer (FRP) offered a capable alternative solution for retrofitting of masonry structures instead of conventional retrofitting techniques such as ferrocement, grout injection, and so on. Unreinforced masonry (URM) walls are the main load-bearing elements of masonry structures and the use of FRP enhances the strength, flexibility, and ductility under earthquake loading. Therefore, techniques of FRP application has become very effective in the strengthening of damaged URM walls. However, the strengthening of masonry structures by means of carbon fibers still lacks adequate theoretical and experimental verification, unlike reinforced concrete (RC) structures. Therefore, attention should be primarily focused on the description of the URM- and FRP-confined wall behavior under shear and compression. This study aims to investigate the finite element analysis (FEA) of URM walls strengthened with FRP composites by adopting an elasto-plastic approach proposed for the assessment of FRP-confined masonry columns under uniaxial compression [1].

A large literature has grown up which extends analytical and numerical models applied to masonry structures. These models involve mechanical parameters that are difficult to measure and cannot be implemented practically into numerical analyses [2–13]. Researchers related to detailed micro-, simplified micro- and macro-FE modeling of masonry walls subjected to compression and shear have initially taken similar steps in the modeling process for masonry prisms and columns under concentric loading. Proceeding in a similar way with that used for the RC members [8, 9, 11, 12] employed a general-purpose finite element program LUSAS [14] for modeling the unreinforced and reinforced masonry prisms and columns activating both the elasto-plastic and isotropic damage models to reflect the nonlinear behavior of the blocks, grout, and mortar joints. Masonry walls were assumed as isotropic and elastic ignoring the influence of mortar joints acting as planes of weakness. The fact that a complete constitutive model should reflect the inelastic material properties of the units and mortar and a failure criterion describing the conditions for failure under combined compression-tension required more detailed analytical studies [15] and experimental investigations [16]. A micro-model should include several material parameters such as modulus of elasticity, Poisson's ratio, cohesion, internal friction angle, and compressive and tensile strength for the representation of units and mortar. Moreover, the composite unit-mortar interface model requires additional material parameters for the description of the interface behavior, for example, tensile strength, cohesion, internal friction angle, compressive strength, tensile fracture energy, shear fracture energy, dilatancy angle, and the close prediction for the experimental load-displacement diagram could be possible in the application of the theoretical model if the shear properties were reduced to 30%, the compressive strength to 20%, and the compressive fracture energy was multiplied by three [17]. From the engineering point of view, there is considerable limitation in the applicability of these sophisticated models [18–23] to FE analysis of masonry walls unless rational relations for the material parameters necessary to explain the models are provided.

The implementation of the plasticity theory to FRP-strengthened masonry walls under vertical and lateral loads by considering the constitutive behavior of masonry units, mortar, and FRP composite material separately, in this study, is analyzed. Köksal et al. [1] considered FRP-confined masonry columns as pressure-dependent material structures based on Drucker-Prager (DP) criterion. A DP-type yield criterion is also employed relating the cohesion and the internal friction angle of both the masonry unit and mortar to their uniaxial compressive strength by extending the previous approach to the FRP-strengthened masonry walls. For this purpose, an extensive parametric study is performed in order to explain the mechanical properties of masonry units and mortar with only one single parameter, that is, their uniaxial compressive strength [24]. Seven masonry walls are considered here. Three of them [25, 26] were unreinforced, single-sided strengthened with glass fiber-reinforced polymer (GFRP), and strengthened by carbon fiber-reinforced polymers (CFRP) strips on one side, respectively. Two of them [27] were strengthened by polyethylene terephthalate (PET) fiber sheets with unidirectional fiber; one was fully wrapped and the other was partially wrapped with both vertical and horizontal strips of PET sheets. One of them [28] was double-sided strengthened with FRP and the other [29] was unreinforced masonry walls, respectively. These seven walls are successively analyzed using FEA method with the proposed approach in LUSAS software [14].

2. The mechanics of constitutive modeling

A large literature has grown up which extends analytical and numerical models applied to masonry structures. These models involve mechanical parameters that are difficult to measure and cannot be implemented practically into numerical analyses. Several experimental and analytical studies on the behavior of masonry shear walls as the main structural component of masonry have been carried out in order to obtain a comprehensive approach for the overall assessment of masonry behavior [18, 21, 30–35]. Proposed theoretical models for implementation to FE analysis of masonry generally require a large number of material parameters that are difficult to measure easily and reliably. For this reason, several attempts have been made to express the stress-strain relationships of the masonry and its constituents using different modeling techniques such as micro-modeling, homogenization approach, and macro-modeling. The common approach in these studies is to treat masonry as a continuous medium or an equivalent continuous medium with the exception of detailed micro-modeling. Detailed micro-modeling should describe the masonry, mortar, and the interaction behavior between them [22, 36–38]. Köksal et al. [1, 8, 9] have performed FE analysis of masonry prisms and columns strengthened with FRP describing the constitutive behavior of the unit, mortar, and FRP separately. The similar approach has been adopted for the FE modeling of masonry shear walls while making the assumption that the material description of the mortar includes the effect of the unit-mortar interface behavior. Since the most common test performed on concrete-like brittle materials is for the measurement of its uniaxial compressive strength, it seems reasonable that the mechanical properties of masonry constituents can be assumed to be related to their compressive strengths. The authors have adopted this strategy in the elasto-plastic analyses of RC elements, masonry prisms, and columns, successively [1, 39, 40].

The most important mechanical parameter in FE analysis for masonry is the modulus of elasticity (E_m) determined by uniaxial compression tests. The failure mechanism and load-displacement behavior of masonry are strongly affected by the differences in the modulus of elasticity between unit and mortar [24, 41]. In detailed micro-modeling, modulus of elasticity of units and mortar are required for NLFEA of the masonry walls. The relations for the masonry constituents are given in **Table 1** [24, 42].

Multi-axial stress states generally define the behavior of the structures such as masonry walls, RC panels, confined columns, or elements loaded over a specified limited area. The basic plastic models, that is, Mohr-Coulomb (MC) and DP are widely adopted in constitutive modeling of frictional materials, like concretes, soils, and rocks, when describing the material behavior beyond the elastic range. Since material parameters of MC criterion are easily obtained from standard tests and are logical from the physical point of view, MC criterion is the most common used criterion in geotechnical and structural engineering [13]. MC criterion in three-dimensional (3D) stress space can be expressed as Eq. (1):

$$f(\xi, \rho, \theta) = \sqrt{2} \xi \sin \phi + \sqrt{3} \rho \sin \left(\theta + \frac{\pi}{3} \right) + \rho \cos \left(\theta + \frac{\pi}{3} \right) \sin \phi - \sqrt{6} c \cos \phi = 0 \quad (1)$$

for $0 < \theta < \frac{\pi}{3}$

where $\xi = I_1/\sqrt{3}$, $\rho = \sqrt{2} J_2$ and $\theta = \arccos \left(\frac{3J_3}{2J_2 \sqrt{3} I_1} \right)$ [43]. The invariants ξ and I_1 indicate the hydrostatic component of the current stress state. However, because of the smooth surface approximation to the six-faceted MC yield function, DP criterion is conversely easy to implement and allows a fast computation of plastic behavior, even it is a drawback from the physical point of view given as Eq. (2) [1, 44]:

$$f(\xi, \rho) = \sqrt{6} \alpha \xi + \rho - \sqrt{2} k = 0 \quad (2)$$

where α and k are material constants. Generally, these constants are expressed in terms of the cohesion (c) and the internal friction angle (ϕ) [13]. Therefore, the surfaces of both DP and MC yield criteria are made to coincide along the compression meridian, and then the constants α and k are related to the constants c and ϕ by [45] given in Eq. (3):

$$\alpha = \frac{2 \sin \phi}{\sqrt{3}(3 - \sin \phi)}, k = \frac{6c \cos \phi}{\sqrt{3}(3 - \sin \phi)} \quad (3)$$

Material	Expression
Brick	$E_{br} = (300 \sim 700) f_{br}$
Block	$E_{bl} = 1000 f_{bl}$
Mortar	$E_{mr} = 200 f_{mr}$

Table 1. Expressions for modulus of elasticity of the masonry constituents.

In masonry columns strengthened with FRP, since the existence of major and intermediate principal stresses σ_1 and σ_2 will affect the yielding and the shape of the deviatoric section, the effect of FRP confinement should be included in the derivation of the material parameters. Due to the complexity of establishing a general failure surface in the principal stress space because of the lack of necessary experimental data, the mean stress $\sigma_m = I_1/3$ at the failure point is defined as a constant value which is corresponding to $(f_{mu} + 2f_l)/3$ at all stress levels. The cohesion and the internal friction angle of the units to include the confinement stresses are given as Eq. (4):

$$\frac{c_{mu}}{f_{mu}} = \frac{\tan \phi_{mu}}{3} \sqrt{\frac{|\sigma_m|}{f_{mu}}} \leq \frac{c_{mu}}{f_{mu}} \left| \frac{\sigma_m}{f_{mu}} \right| = 1 \quad (4)$$

$$\phi_{mu} = \phi_i - 0.75 \frac{|\sigma_m|}{f_{mu}} \geq \phi_f = \phi_{mu} \left| \frac{I_1}{f_{mu}} \right| = 1 \quad (5)$$

In Eq. (5), ϕ_i can be nearly equal to $\pi/3$ for brick and $\pi/4$ for concrete. Besides, applying the boundary condition, ϕ_f is approximately $\pi/4$ for brick and between $\pi/5$ and $\pi/6$ for concrete. For high hydrostatic pressures ($0 > \sigma_m/f_{mu} \geq -1$), internal friction angle can be taken as a constant value, that is, 30° – 35° for concrete and nearly 45° for clay brick as illustrated in **Figure 1**. Since much lower pressures exist on masonry walls and their constituents, material parameters have been calibrated to best reconcile the experimental data of several walls. In the wall tests, as the axial load level is less than the ultimate uniaxial strength, the mean stress can be taken as a constant value corresponding to $(p + 2f_l)/3$ at all stress levels. The validity of Eqs. (4) and (5) is finally verified by numerical simulations of the walls subjected to the pressures in the range of $\xi/f_{mu} \leq -0.58$ throughout this study.

The use of the compressive meridian obviously causes some overestimation for the failure load for this case. In order to lessen this overestimation, an ending point definition for the termination of NLFEA should be needed. The ending point for the analysis can be determined

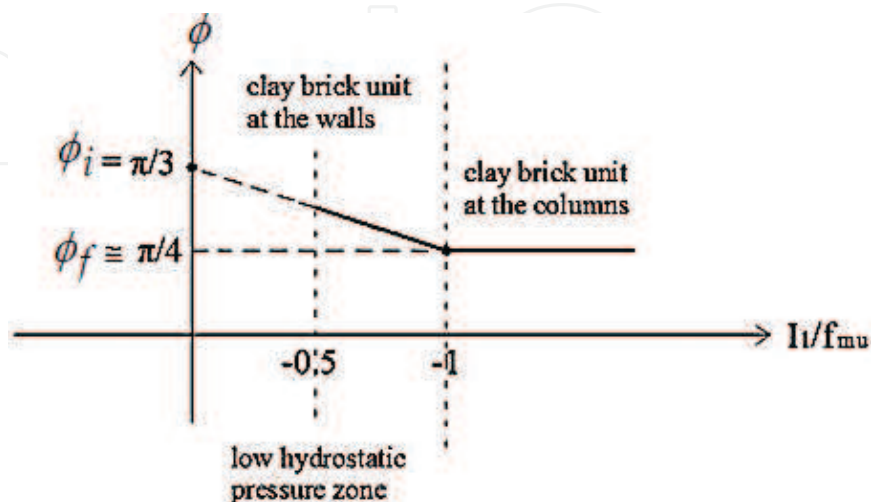


Figure 1. Plotting of Eq. (5) for the internal friction angle of clay brick [13].



Figure 2. Assumption for the discontinuity surface between two units along the thickness of the mortar resulting failure of the wall [13].

defining the discontinuity surface between two units along the thickness of the mortar as illustrated in **Figure 2**. The maximum tensile strain can then be determined from the case of that a complete opening will occur along the mortar thickness between two units as given in Eq. (6):

$$\varepsilon_{\max} = h_{mr} / (2h_{br} + h_{mr}) \quad (6)$$

Mortar generally governs the nonlinear behavior of masonry and has an influence on the axial strain of masonry prism and also on the shear response of the masonry walls [24, 46]. Therefore, any theoretical model should account for the nonlinear response of both the mortar and the unit-mortar interface to predict the inelastic behavior of masonry [41, 47]. In this study, the mechanical parameters of mortar, given in Eqs. (7) and (8), are adjusted to reflect the unit-mortar interface response as preferred in the modeling of masonry prisms and columns previously [1, 8]:

$$c_{mr} = 1.55 \sqrt[3]{f_{mr}} \quad (7)$$

$$\phi_{mr} = 1.519 f_{mr} \quad (8)$$

3. Finite element modeling and model verification

Three-dimensional (3D) finite element models for masonry walls strengthened with FRP composites are developed in LUSAS [14]. Masonry constituents, that is, brick and mortar, are assumed to be isotropic elasto-plastic obeying DP criterion. They are modeled separately with eight-noded hexahedral element (HX8M) which is a solid element with an incompatible strain field as illustrated in **Figure 3a**. FRP composites are modeled by four-noded thick shell element (QTS4) which has a thick and thin curved shell geometry including multiple branched junctions as in **Figure 3b**. Both the element formulations take account of membrane, shear and flexural deformations, and are capable of modeling inelastic phenomenon.

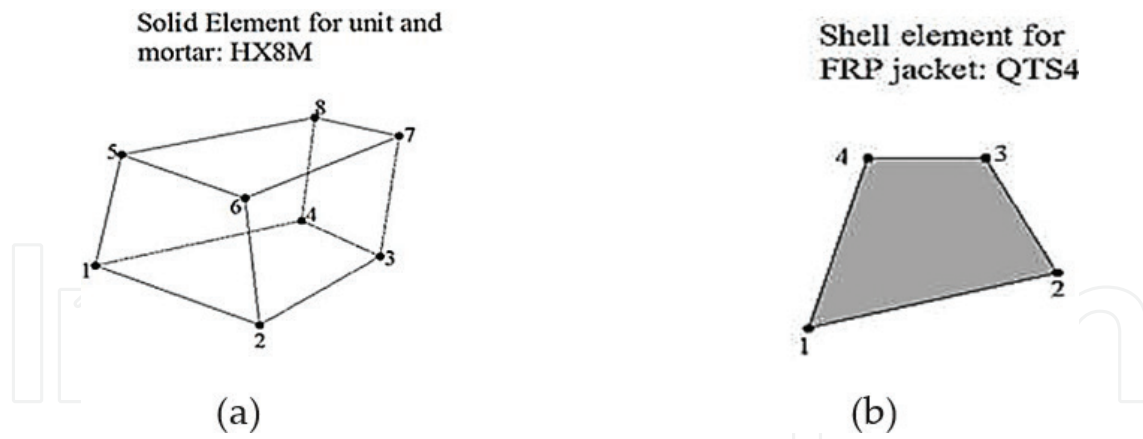


Figure 3. (a) Eight-noded hexahedral element for units and mortar and (b) four-noded thick shell element for FRP jacket [13].

Table 2 shows the material and geometrical properties for masonry walls with its FRP confinement evaluated in this study. All mechanical properties of the masonry constituents utilized in the analyses are also given in Table 3.

Stratford et al. [25] tested six 1200×1200 mm masonry panels under a combination of vertical preloading, and in-plane horizontal shear loading. Both clay and concrete brick specimens were tested while one specimen of each material was left unreinforced and the other two panels were single-sided strengthened using GFRP. GFRP had equal amounts of fibers in the horizontal and vertical directions (parallel to the mortar joints) and fibers were oriented at 45° to the joints. As can be seen in Figure 4, two connected hydraulic jacks (N) were placed on the wall while the shear load was applied to the wall by a horizontal hydraulic jack (P).

For the case of URM wall, the end point for the FEA is determined defining a discontinuity surface between two clay units along the thickness of the mortar. The maximum tensile strain pointing out that a complete opening will occur along the mortar thickness between two units, can be found by dividing the mortar joint thickness 10 mm by two block heights plus the mortar thickness as $10/(2 \times 65 + 10) = 0.071$. This strain value can be called critical tensile strain. As the lateral load is increased, the effect of tensile deformations grows up along the toe of the wall and it is easy to observe the critical tensile strain at the toe of the wall from Figure 5. If FEA ends when the ultimate tensile strain at the wall reaches the critical value, both simulation model and laboratory test results agreed very well as shown in Figure 6.

As can be seen in Figure 6, horizontal displacement at the failure is experimentally determined approximately as 14 mm. NLFEA gives a value of 13.81 mm from the use of the maximum tensile strain criterion for the wall. As can be seen in Figures 5 and 7, the region of concentrated maximum tensile strain matches the location of experimental crack pattern on the wall.

Figure 8 shows the stress-strain plots for strengthened wall Clay 2. The load-displacement plot obtained from NLFEA is well agreed with the experimental data. As shown in Figure 9, the analysis is terminated upon reaching the maximum tensile strain corresponding to the tensile strength of GFRP at a horizontal drift of 10.16 mm. This value is experimentally determined approximately as 12 mm.

Reference	Experiment	Precompression load (MPa)	Wall dimension (mm)	Brick dimension (mm)	FRP	
					E_{FRP} (MPa)	t (mm)
Stratford [25]	Clay 1 URM	1.38	1200 × 1200 × 60	228 × 65 × 60	-	-
	Clay 2 GFRP	1.38	1200 × 1200 × 60	228 × 65 × 60	73,300	0.15
Capozucca [26]	HRM-C2	1.5	840 × 633 × 50	100 × 17 × 50	240,000	0.177
Rahman and Ueda [27]	WALL 3	1.16	860 × 540 × 100	205 × 60 × 100	10,000	0.841
	WALL 4					
Mosallam and Banerjee [28]	W4-C-RT	1.29	1830 × 1830 × 203	406 × 152 × 203	96,500	1.60
Haider [29]	URM 6	0.5	2870 × 2408 × 150	310 × 76 × 150	-	-

Table 2. General characteristics of masonry walls and FRP confinement.

Reference	Experiment	Brick			Mortar		
		E_{mu} (MPa)	c_{mu} (MPa)	ϕ_{mu} (°)	E_{mr} (MPa)	c_{mr} (MPa)	ϕ_{mr} (°)
Stratford [25]	Clay1 URM	18,600	3.04	59.68	3250	3.45	16.71
	Clay 2 GFRP	18,600	3.04	59.68	3250	3.45	16.71
Capozucca [26]	HRM-C2	7000	2.33	59.37	150	2.21	4.41
Rahman and Ueda [27]	WALL 3	8000	2.27	58.94	125	12.5	18.90
	WALL 4	8000	2.16	59.06	125	12.5	18.90
Mosallam and Banerjee [28]	W4-C-RT	6000	2.32	57.66	800	3.79	22.20
Haider [29]	URM 6	20,000	0.90	59.54	1100	2.65	7.59

Table 3. Mechanical properties adopted for FE analyses.

In all experiments, except for the unreinforced clay specimen (Clay 1), the strengthened masonry walls (Clay 2) failed by rapid propagation of diagonal crack which followed the mortar joints as in **Figure 10a**. Crushing failure, which occurred when the compressive strength of the mortar was reached, cannot happen for these walls because of the mortar strength higher than 11 MPa. Shear failure, involving sliding along a slip plane either within the mortar or at the brick-mortar interface, is the main failure mode. The fracture pattern is well predicted through the concentration of the maximum tensile strains diagonally shown in **Figure 10b**.

Capozucca [26] investigated the behavior of historical reinforced masonry (HRM) walls strengthened by CFRP strips, experimentally. CFRP strips bonded to only one face of the specimen horizontally and vertically. FRP strips, containing unidirectional fibers, can be bonded to the surface of the wall and arranged to provide an external truss action [25]. The

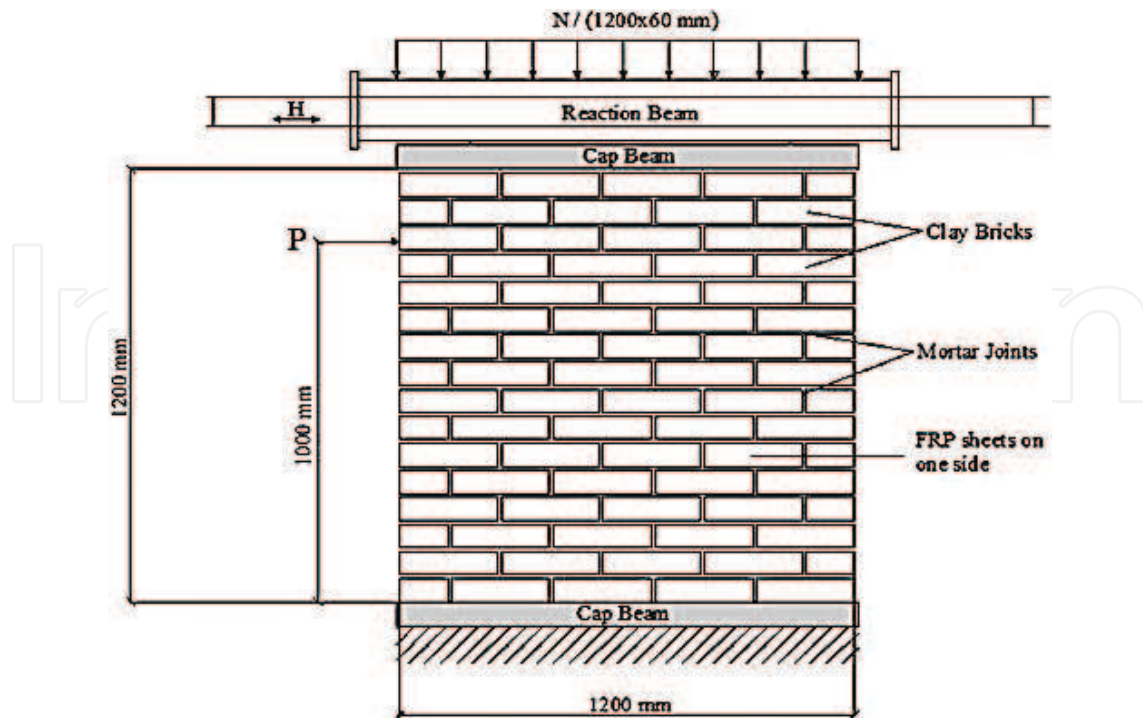


Figure 4. Experimental setup of shear wall Clay 2 [13].

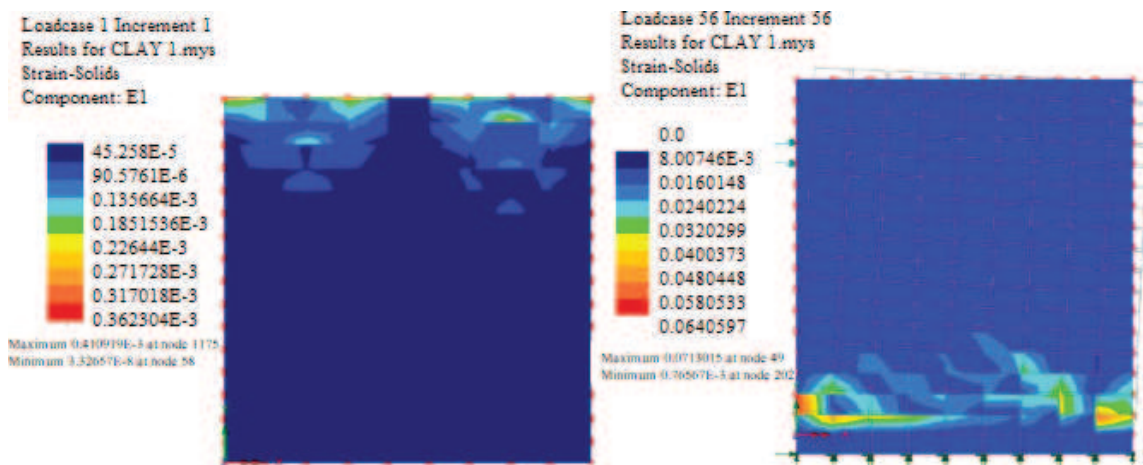


Figure 5. Maximum strains along the wall height for Clay 1 [13].

strengthened wall was subjected to cyclic loading until failure. Specimens were built with clay bricks and mortar with thickness 4 mm. Flexural tensile strength of mortar was 0.80 MPa. A single-story HRM C2 wall was built using historic full clay bricks in scale, one-third, and was tested in a special frame (Figure 11). Besides, mechanical and geometrical properties of brick, mortar and CFRP strips are given here in Tables 2 and 3.

Initially, pre-compression load (1.50 MPa) was applied to the flanges and web by three jacks, kept constant, then horizontal force was applied measuring horizontal force until failure [26]. Wall C2 damaged by cyclic shear tests and then was strengthened by 50 mm wide carbon strips

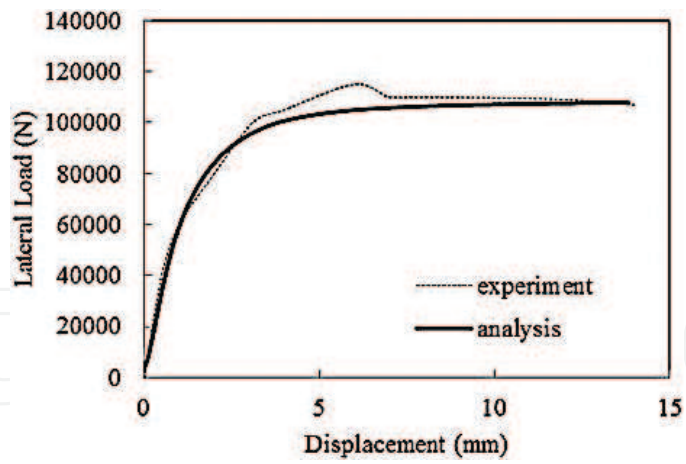


Figure 6. Lateral load-displacement responses for Clay 1 [13].

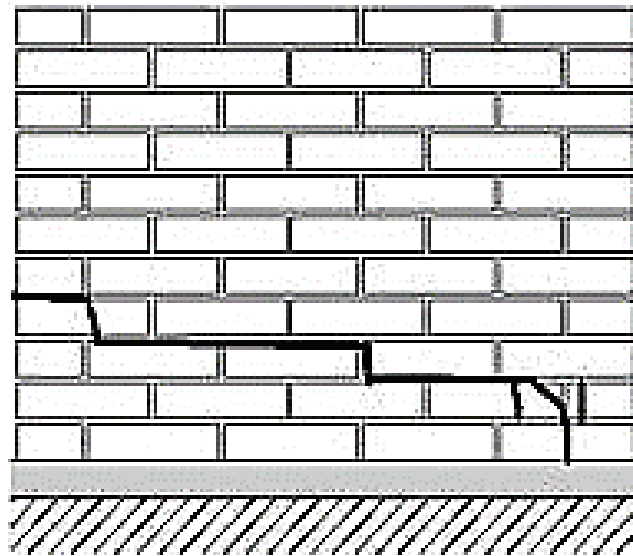


Figure 7. Experimental crack pattern for Clay 1 [13].

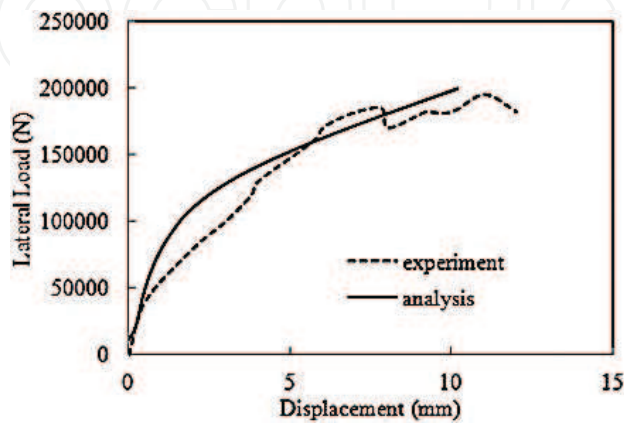


Figure 8. Lateral load-displacement responses for strengthened Clay 2 [13].

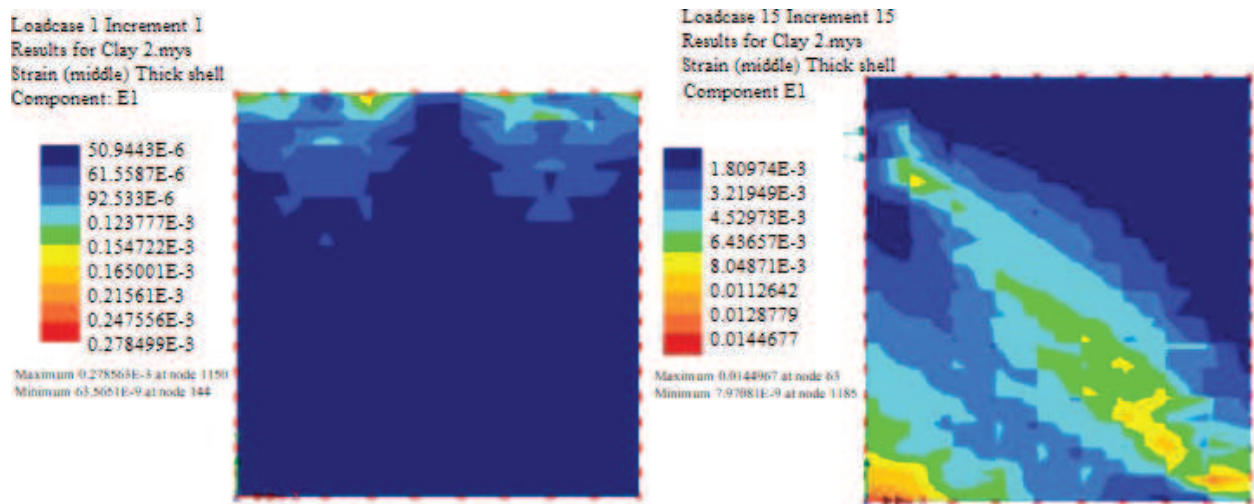


Figure 9. Maximum strain distribution over GFRP surface [13].

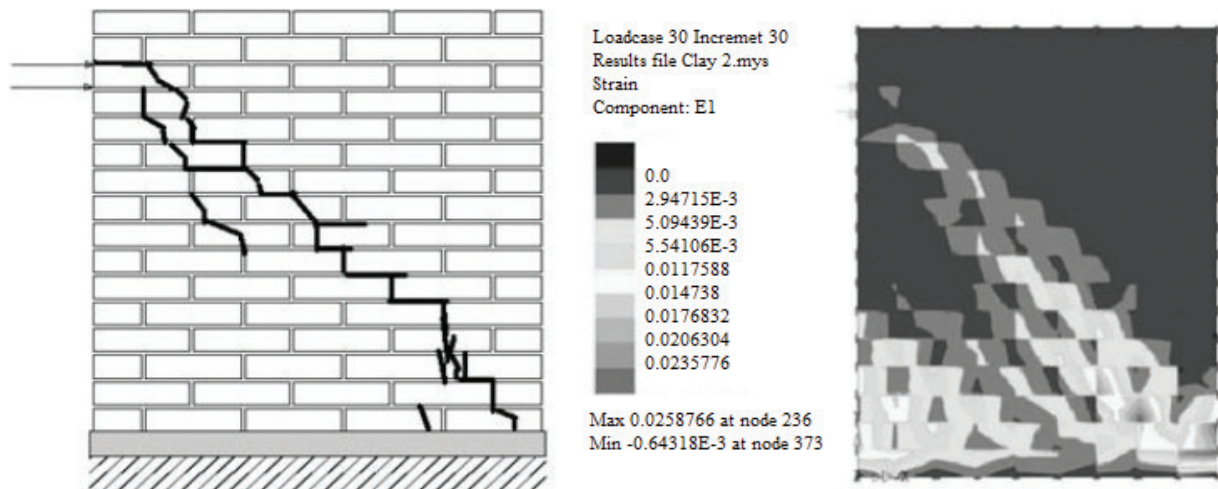


Figure 10. (a) Schematic crack patterns in strengthened wall (Clay 2) and (b) maximum tensile strains over unreinforced face in 3D FE model [13].

bonded to one side, parallel and normal to mortar joints. Mechanical parameters of CFRP strips are summarized in **Table 2**. Walls C1 and C2 were initially subjected, respectively, to five cyclic stages of horizontal force and seven cyclic stages before to bring the walls to failure by an ultimate stage with unidirectional horizontal force [26]. These are the possible reasons for the stiffer behavior observed in **Figures 12** and **13**. The critical tensile strain assumption for masonry is adopted for the stress-strain plots (**Figure 13**), while the analysis is terminated by reaching the tensile strength of GFRP as in **Figure 12**. Therefore, the material parameters for the masonry constituents of the pre-damaged walls should be somewhat lower than the recommended ones in Eqs. (4)–(7). The cohesion and internal friction angle values of the clay brick lowered by 35 and 15%, respectively. Since the mortar has already defined by a very weak material, any reduction on its mechanical properties will not be reasonable. Another reason for the stiffer predictions can be the present approach does not consider the debonding

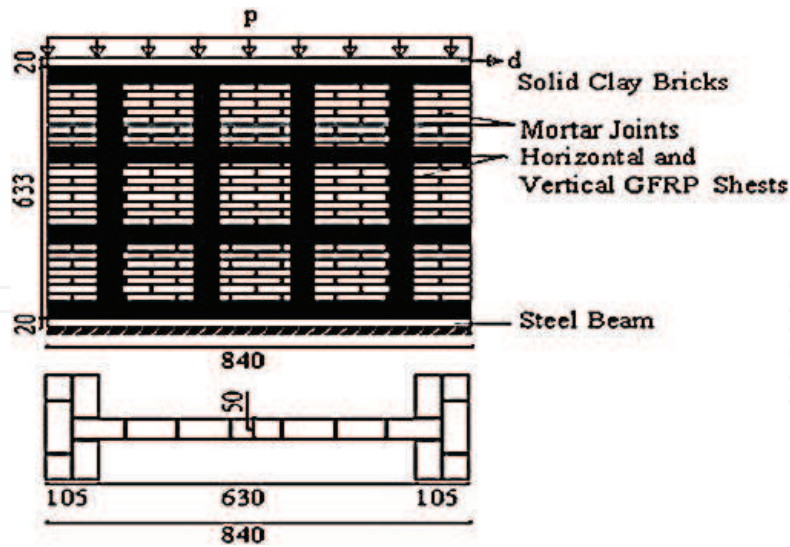


Figure 11. Geometrical details of HRM C2 wall [13, 26].

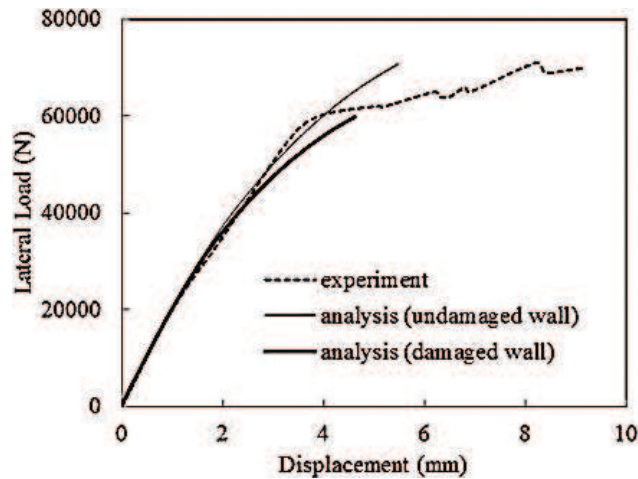


Figure 12. Comparison of load-displacement responses for pre-damaged HRM C2 wall employing the ultimate tensile strain criterion of GFRP [13].

phenomenon between the wall and FRP layer which affects the maximum lateral displacement of the wall particularly while reaching the ultimate load capacity [48].

Actually, presence of discontinuity surfaces with some specific values of separation affects the failure mechanisms and the level of FRP confinement in cracked and damaged walls. Therefore, the use of the critical tensile strain criterion instead of the ultimate tensile strength of FRP can be more reasonable for the analysis of pre-damaged walls.

Rahman and Ueda [27] studied the mechanical behavior of masonry walls experimentally. WALLS 1 and 2 were unreinforced, and WALLS 3 and 4 were fully (%100) and partially (%40) strengthened with FRP, respectively (Figure 14). The dimensions of each brick unit were 205 × 100 × 60 mm while the dimensions of walls were 860 × 540 × 100mm with an approximate mortar thickness of 10 mm. A pre-compression of 100 kN (1.16 MPa) was

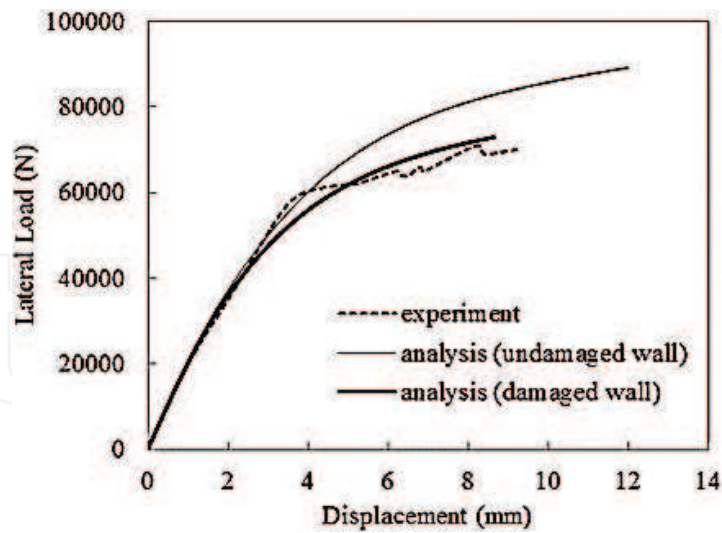


Figure 13. Comparison of load-displacement responses for pre-damaged HRM C2 wall adopting the maximum tensile strain criterion of masonry [13].

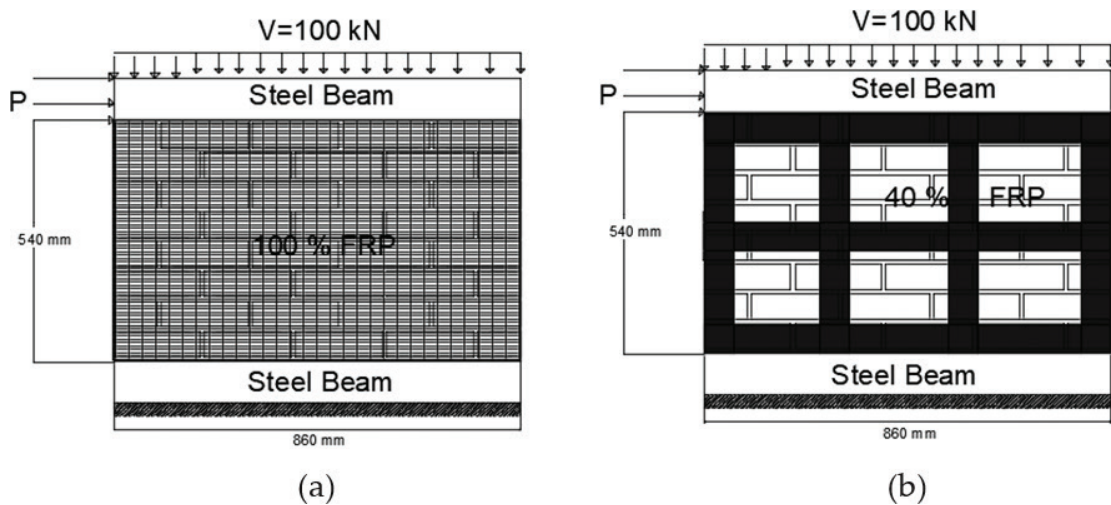


Figure 14. Geometrical details of experiments (a) WALL 3 and (b) WALL 4 [27].

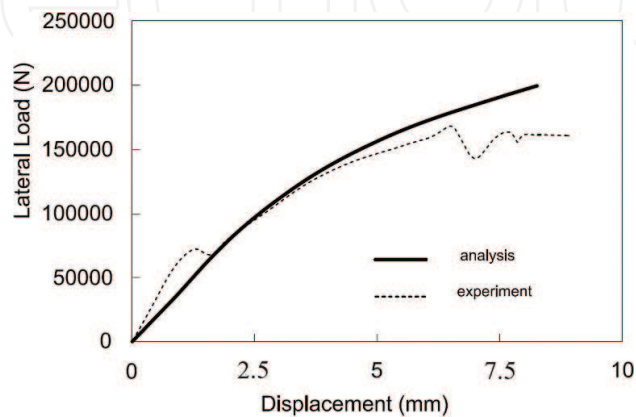


Figure 15. Comparison of load-displacement responses for WALL 3.

applied on the top of the wall. The modulus of elasticity and the tensile strength of FRP sheet were 10,000 and 740 MPa, respectively [49].

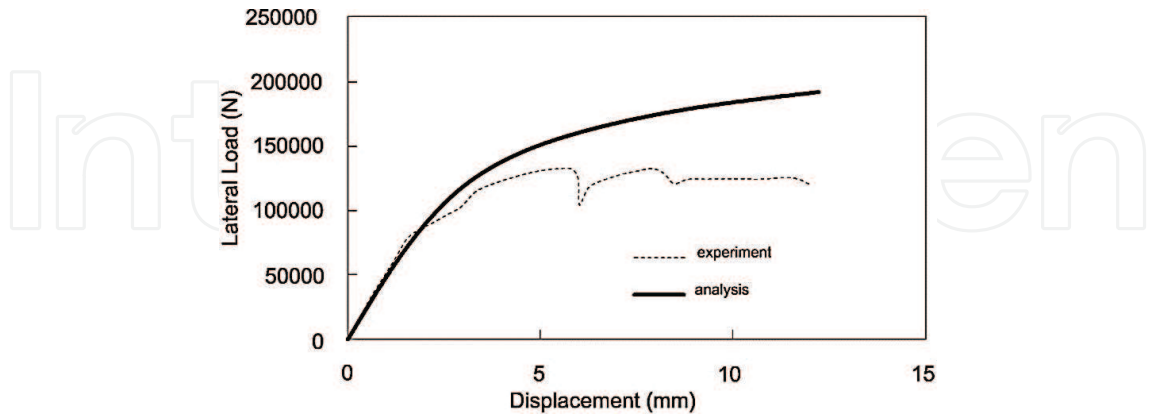


Figure 16. Comparison of load-displacement responses for WALL 4.

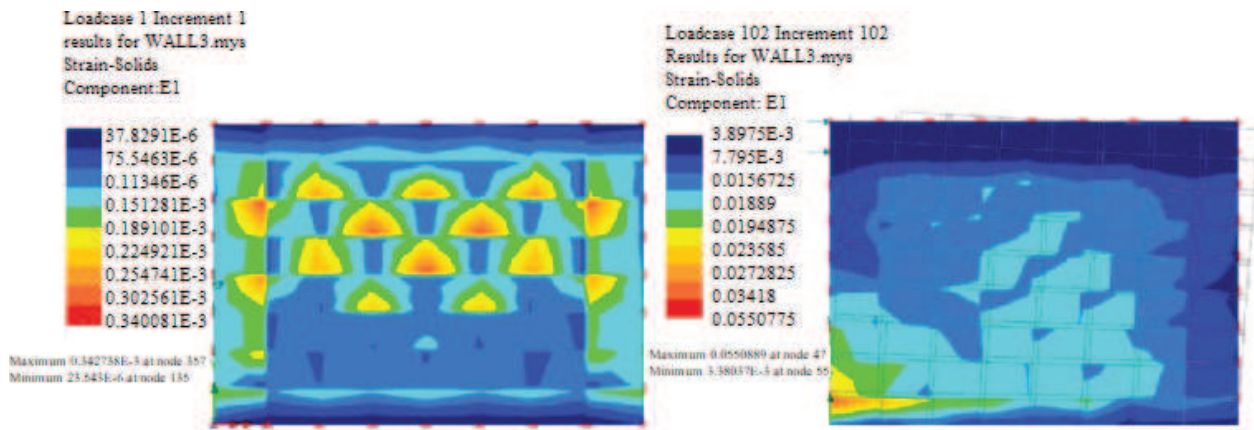


Figure 17. Maximum strains along the height of WALL 3.

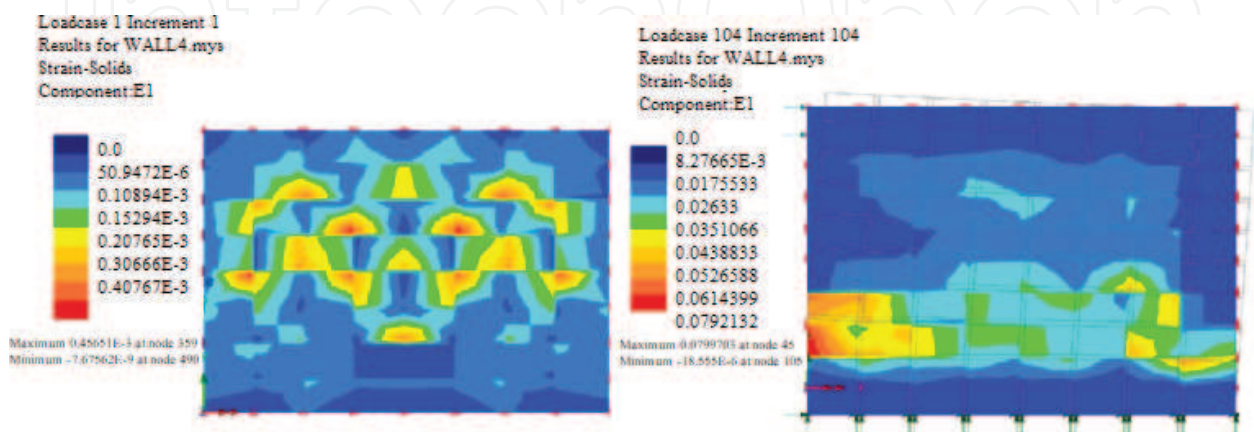


Figure 18. Maximum strains along the height of WALL 4.

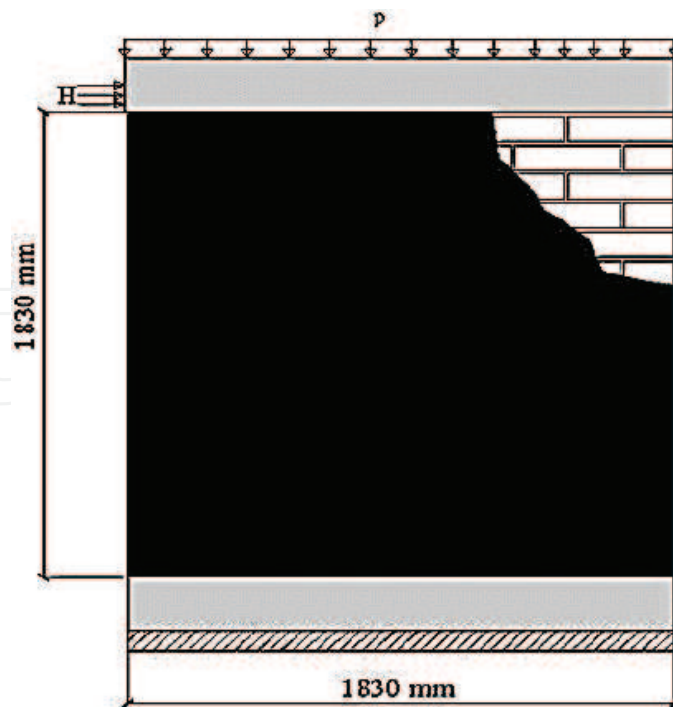


Figure 19. Experimental setup of W4-C-RT wall.

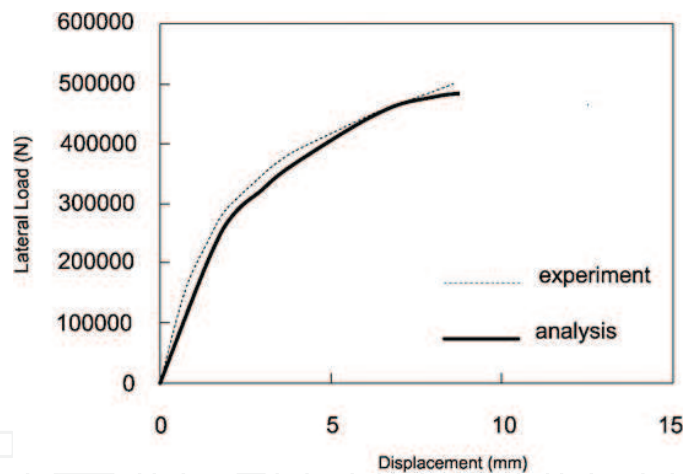


Figure 20. Lateral load-displacement responses for W4-C-RT.

The stress-strain plots for WALL 3 are shown in **Figure 15**. The load-displacement plot (**Figure 16**) obtained from NLFEA is well agreed with the experimental data. The analysis is terminated upon reaching the maximum tensile strain corresponding to the tensile strength of PET at a horizontal drift of 8.80 mm for WALL 3 (**Figure 17**). This value is experimentally determined approximately as 9.30 mm. Finally, the maximum strains along the wall height are depicted in **Figure 17**. The analysis is terminated upon reaching the maximum tensile strain corresponding to the tensile strength of PET at a horizontal drift of 12.50 mm (**Figure 18**). This value is experimentally determined approximately as 12.40 mm for WALL 4. In **Figure 18**, the maximum strains along the wall height can be seen.

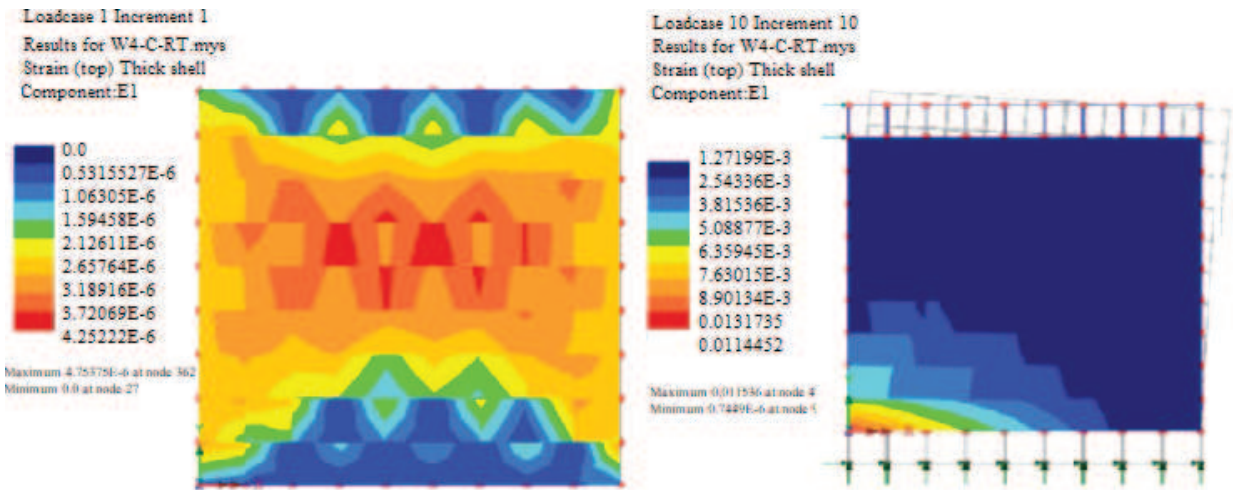


Figure 21. Maximum strains along the wall height (W4-C-RT).

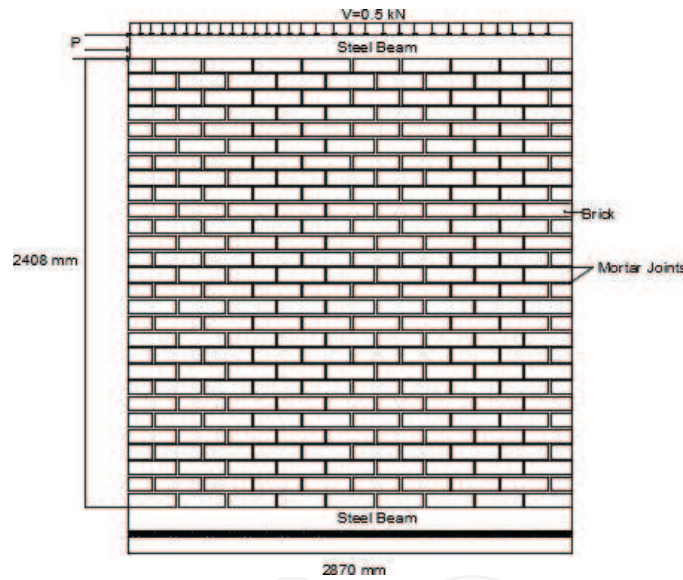


Figure 22. Experimental setup of URM 6 wall.

Mosallam and Banerjee [28] tested six identical masonry wall specimens of size 1830×1830 mm with $406 \times 152 \times 203$ mm hollow concrete block under a combination of constant axial and incremental lateral loads (push-pull) (Figure 19). Two of them were unreinforced and the others were strengthened with different types of FRP elements. The compressive strength of masonry prisms, grout cylinders, and mortar cylinders was calculated as 2.16, 18.96, and 14.62 MPa, respectively. The tensile strength of FRP was 1061 MPa and modulus of elasticity was 96,500 MPa. In this study, W4-C-RT wall retrofitted wall specimen with double-sided carbon/epoxy laminate is considered. The rupture strain of FRP element is calculated as 0.011 from ratio of tensile stress of FRP to modulus of elasticity. Load-displacement curves obtained from experiments and numerical analysis are given in Figure 20.

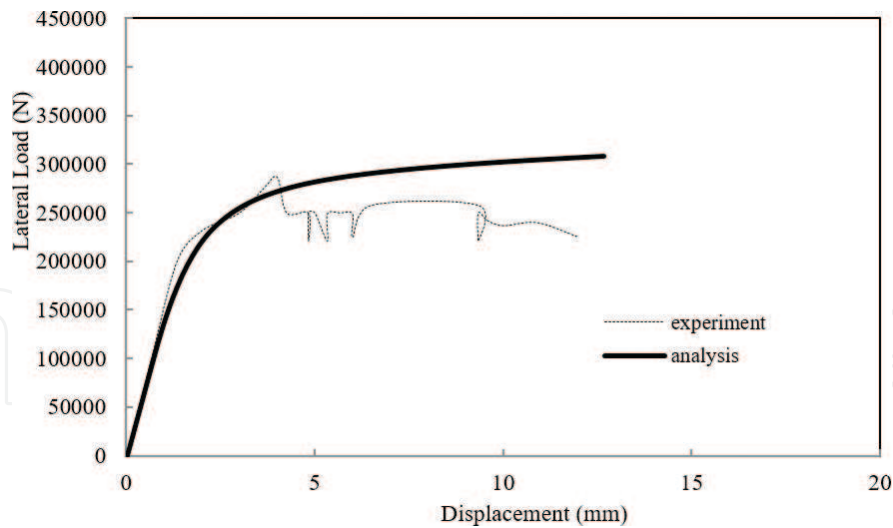


Figure 23. Lateral load-displacement responses for URM 6.

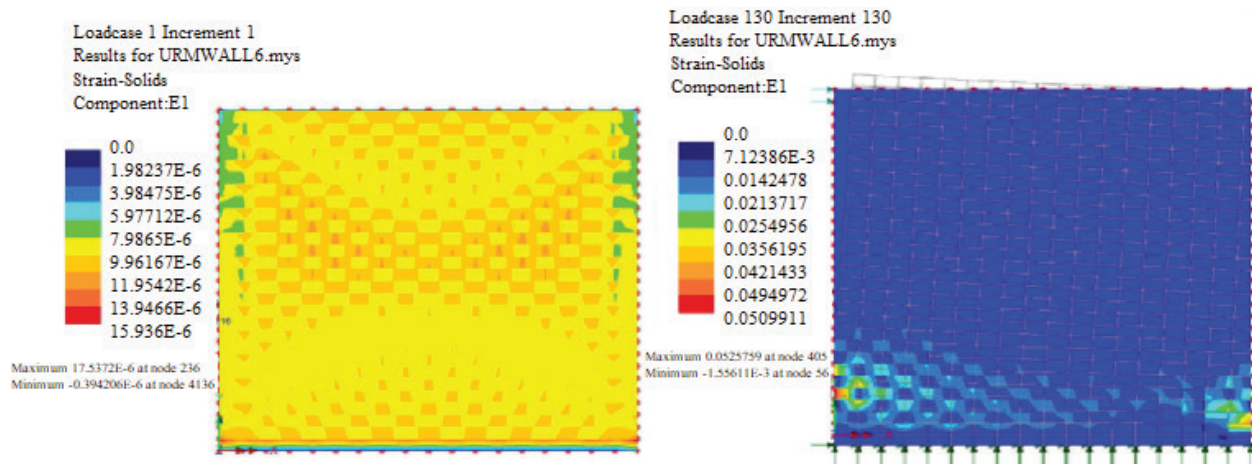


Figure 24. Maximum strains along the wall height (URM 6).

The load-displacement plot obtained from NLFEA is well agreed with the experimental data. As shown in **Figure 21**, the analysis is terminated upon reaching the maximum tensile strain corresponding to the tensile strength of FRP at a horizontal drift of 8.20 mm. This value is experimentally determined approximately as 8.00 mm. The critical tensile strain is calculated as 0.038. As the lateral load is increased, the effect of tensile deformations grows up along the toe of the wall and it is easy to observe the critical tensile strain at the toe of the wall from **Figure 21**.

Haider [29] investigated the behavior of clay brick masonry walls under a combination of vertical preloading, and lateral shear loading (**Figure 22**). Mechanical and geometrical properties of brick and mortar are given in **Table 3**. Compressive strength of clay brick and mortar were 15.7 and 5.00 MPa, respectively. For the case of clay brick masonry wall, the end point for the

FEA is determined defining a discontinuity surface between two brick units along the thickness of the mortar. The maximum tensile strain can be found as 0.061. Load-displacement curve obtained from NLFEA and experimental data is given in **Figure 23**.

As shown in **Figure 24**, the analysis is terminated upon reaching the maximum tensile strain at a horizontal drift of 13.00 mm. Experimental value is approximately as 12.40 mm. The effect of tensile deformations grows up along the toe of the wall under increasing lateral load and the critical tensile strain is observed at the toe of the wall (**Figure 24**).

4. Conclusions

This chapter deals with the implementation of the plasticity theory to URM and FRP-strengthened masonry walls under compression and shear by considering the constitutive behavior of masonry units, mortar, and FRP composite material separately. A DP-type yield criterion is also employed relating the cohesion and the internal friction angle of both unit and mortar to their uniaxial compressive strength by extending the previous approach to the FRP-strengthened masonry walls. For this purpose, a large parametric study is performed in order to explain the mechanical properties of unit and mortar with only a single parameter, that is, their uniaxial compressive strength [24]. In order to evaluate the accuracy of the proposed approach, the analytical results are compared with the experimental results of both unreinforced and strengthened masonry walls tested in two different experimental studies. Following conclusions are drawn:

1. The analytical approach previously recommended for masonry columns for the cohesion and internal friction angle have been updated and extended to the analysis of FRP-strengthened URM walls. The behavior of URM as well as the FRP-confined masonry walls simulated by means of the proposed approach considering these analytical relations is consistent with the test results.
2. Elasto-plastic analyses need an ending-point definition to terminate NLFEA when the stress-strain curve has an ideal plastic plateau. For the case of URM wall, the end point is determined defining the discontinuity surface between two clay units along the thickness of the mortar. It is possible to calculate the maximum strain ε_t by dividing the mortar thickness by two block heights plus the mortar thickness. FEA should be interrupted when the ultimate tensile strain at the wall reaches this value. For the case of strengthened walls with FRP, FEA can be interrupted when the ultimate tensile strain reaches the rupture strain, $\varepsilon_{rup} = f_t/E_{FRP}$. For the analyses of both the strengthened walls which are previously tested and damaged ones, and the employment of FRP strips which confines only to one side of the wall partially, the use of the maximum tensile strain criterion of masonry seems much more reasonable.
3. Cohesion and internal friction values of the masonry units are expressed in terms of hydrostatic pressure at the failure and their uniaxial compressive strength. The relations of masonry constituents are recommend are valid for $\xi/f_{mu} < 0.58$. The dependency of the material parameters of the frictional materials on the hydrostatic pressure is then reflected into the analysis directly.

4. The material parameters of DP criterion are expressed in terms of the cohesion and the internal friction angle of MC criterion in this study. Therefore, the surfaces of both DP and MC yield criteria are made to coincide along the compression meridian.

Nomenclature

c	cohesion
c_{mr}	cohesion of mortar
E_{bl}	modulus of elasticity of the blocks
E_{br}	modulus of elasticity of bricks
E_m	modulus of elasticity
E_{mr}	modulus of elasticity of the mortar
f_{bl}	compressive strength of the blocks
f_{br}	compressive strength of bricks
f_l	confining pressure exerted by FRP
f_{mr}	compressive strength of the mortar
f_{mu}	uniaxial compressive strength of the unit
h_{br}	height of the unit
h_{mr}	height of the mortar thickness
I_1	first invariant of the stress and the deviatoric tensor
J_2	second invariant of the stress and the deviatoric tensor
k	material constant
p	vertical pre-compression of the wall
α	material constant
ε_{max}	maximum tensile strain
ξ	hydrostatic component of the current stress state
ϕ	internal friction angle
ϕ_i	initial angle of internal friction in radians
ϕ_f	final angle of internal friction in radians
ϕ_{mr}	internal friction angle of mortar
σ_m	mean stress

Author details

Bilge Doran^{1*}, Hasan Orhun Köksal², Selen Aktan², Oktay Jafarov³ and Cengiz Karakoç⁴

*Address all correspondence to: doranbilge@gmail.com

1 Yıldız Technical University, Istanbul, Turkey

2 Çanakkale Onsekiz Mart University, Çanakkale, Turkey

3 WorleyParsons Baku Office, Azerbaijan

4 Boğaziçi University, Istanbul, Turkey

References

- [1] Köksal HO, Aktan S, Kuruşçu AO. Elasto-plastic finite element analysis of FRP-confined masonry columns. *Journal of Composites for Construction*. 2012;**16**(4):407-417. DOI: 10.1061/(ASCE)CC.1943-5614.0000268
- [2] Hamid AA, Chukwunenye AO. Compression behavior of concrete masonry prisms. *Journal of Structural Engineering*. 1986;**112**(3):605-613. DOI: 10.1061/(ASCE)0733-9445(1986)112:3(605)
- [3] Cheema TS, Klingner RE. Compressive strength of concrete masonry prisms. *Journal of the American Concrete Institute*. 1986;**83**(1):88-97
- [4] Khalil MRA, Shrive NG, Ameny P. 3 dimensional stress-distribution in concrete masonry prisms and walls. *Magazine of Concrete Research*. 1987;**39**(139):73-82. DOI: 10.1680/mac.1987.39.139.73
- [5] Ganesan T, Ramamurthy K. Behavior of concrete hollow-block masonry prisms under axial-compression. *Journal of Structural Engineering*. 1992;**118**(7):1751-1769. DOI: 10.1061/(ASCE)0733-9445(1992)118:7(1751)
- [6] Ramamurthy K. Behavior of grouted concrete hollow block masonry prisms. *Magazine of Concrete Research*. 1995;**47**(173):345-354. DOI: 10.1680/mac.1995.47.173.345
- [7] Sayed Ahmed EY, Shrive NG. Nonlinear finite-element model of hollow masonry. *Journal of Structural Engineering*. 1996;**122**(6):683-690. DOI: 10.1061/(ASCE)0733-9445(1996)122:6(683)
- [8] Köksal HO, Doran B, Ozsoy AE, Alacalı SN. Nonlinear modeling of concentrically loaded reinforced blockwork masonry columns. *Canadian Journal of Civil Engineering*. 2004;**31**(6):1012-1023. DOI: 10.1139/104-058
- [9] Köksal HO, Karakoç C, Yıldırım H. Compression behavior and failure mechanisms of concrete masonry prisms. *Journal of Materials in Civil Engineering*. 2005;**17**(1):107-115. DOI: 10.1061/(ASCE)0899-1561(2005)17:1(107)

- [10] Shing PB, Lofti HR, Barzegarmehrabi A, Brunner J. Finite-element analysis of shear resistance of masonry wall panels with and without confining frames. *Proceedings of the Tenth World Conference on Earthquake Engineering*. 1992:2581-2586
- [11] Köksal HO, Karakoç C. An isotropic damage model for concrete. *Materials and Structures*. 1999;**32**(222):611-617. DOI: 10.1007/BF02480497
- [12] Köksal HO, Arslan G. Damage analysis of RC beams without web reinforcement. *Magazine of Concrete Research*. 2004;**56**(4):231-241. DOI: 10.1680/macr.2004.56.4.231
- [13] Köksal HO, Jafarov O, Doran B, Aktan S, Karakoç C. Computational material modeling of masonry walls strengthened with fiber reinforced polymers. *Structural Engineering and Mechanics*. 2013;**48**(5):737-755. DOI: 10.12989/sem.2013.48.5.737
- [14] LUSAS Finite Element System, Version 14.5-2. FEA Ltd, Surrey. UK; 2011
- [15] Dhanasekar M, Page AW, Kleeman PW. A finite element model for the in-plane behavior of brick masonry. *Proceedings of the 9th Australasian Conference on Mechanisms of Structures*. 1984:262-267
- [16] Ganz HR, Thurlimann B. Strength of brick walls under normal force and shear. *Proceedings of the 8th International Symposium on Load Bearing Brickwork*. London, U.K; 1983
- [17] Lourenco PB. Computational strategies for masonry structures [Ph.D. thesis]. *Civil Engineering and Geosciences*. Eindhoven, Netherland: Delft University; 1996
- [18] Chaimoon K, Attard MM. Modeling of unreinforced masonry walls under shear and compression. *Engineering Structures*. 2007;**29**(9):2056-2068. DOI: 10.1016/j.engstruct.2006.10.019
- [19] Giambanco G, Rizzo S, Spallino R. Numerical analysis of masonry structures via interface models. *Computer Methods in Applied Mechanics and Engineering*. 2001;**190**(49-50): 6493-6511. DOI: 10.1016/S0045-7825(01)00225-0
- [20] Lourenco PB, Rots JG. Multisurface interface model for analysis of masonry structures. *Journal of Engineering Mechanics*. 1997;**123**(7):660-668. DOI: 10.1061/(ASCE)0733-9399(1997)123:7(660)
- [21] Formica G, Sansalone V, Casciaro R. A mixed solution strategy for the nonlinear analysis of brick masonry walls. *Computer Methods in Applied Mechanics and Engineering*. 2002;**191**(51-52):5847-5876. DOI: 10.1016/S0045-7825(02)00501-7
- [22] Milani G. 3D FE limit analysis model for multi-layer masonry structures reinforced with FRP strips. *International Journal of Mechanical Sciences*. 2010;**52**(6):784, 004-803. DOI: 10.1016/j.ijmecsci.2010
- [23] Grande E, Milani G, Sacco E. Modelling and analysis of FRP-strengthened masonry panels. *Engineering Structures*. 2008;**30**(7):1842-1860. DOI: 10.1016/j.engstruct.2007.12.007
- [24] Jafarov O. Lifli Polimerle Güçlendirilmiş Yığma Duvarların Modellenmesi [Ph.D. thesis]. Istanbul: Civil Engineering, Yıldız Technical University; 2012

- [25] Stratford T, Pascale G, Manfroni O, Bonfiglioli B. Shear strengthening masonry panels with sheet glass-fiber reinforced polymer. *Journal of Composites for Construction*. 2004;**8**(5):434-443. DOI: 10.1061/(ASCE)1090-0268(2004)8:5(434)
- [26] Capozucca R. Experimental analysis of historic masonry walls reinforced by CFRP under in-plane cyclic loading. *Composite Structures*. 2011;**94**(1):277-289. DOI: 10.1016/j.compstruct.2011.06.007
- [27] Rahman A, Ueda T. Numerical simulation of FRP retrofitted laterally loaded masonry. Eleventh North American Masonry Conference. Minneapolis; 5-8 June 2011
- [28] Mosallam A, Banerjee S. Enhancement in in-plane shear capacity of unreinforced masonry (URM) walls strengthened with fiber reinforced polymer composites. *Composites: Part B*. 2011;**42**(6):1657-1670. DOI: 10.1016/j.compositesb.2011.03.015
- [29] Haider W. In plane response of wide spaced reinforced masonry shear walls [Ph.D thesis]. Emerald, Australia: Central Queensland University; 2007
- [30] Krstevska L, Tashkov LJ, Arun G, Aköz F. Evaluation of seismic behavior of historical monuments. SHH07 International Symposium on Studies on Historical Heritage Symposium Book. Antalya, Turkey; 2007. pp. 411-418
- [31] Mele E, De Luca A, Giordano A. Modelling and analysis of a basilica under earthquake loading. *Journal of Cultural Heritage*. 2003;**4**(4):355-367. DOI: 10.1016/j.culher.2003.03.002
- [32] Berto L, Saetta A, Scotta R, Vitaliani R. An orthotropic damage model for masonry structures. *International Journal for Numerical Methods in Engineering*. 2002;**55**(2):127-157. DOI: 10.1002/nme.495
- [33] Tasnimi AA, Farzin M. Inelastic behavior of RC columns under cyclic loads, based on cohesion and internal friction angle of concrete. *Modarres Technical and Engineering Journal*. 2006;**23**:29-40
- [34] Mohebkah A, Tasnimi AA, Moghadam HA. Nonlinear analysis of masonry-infilled steel frames with openings using discrete element method. *Journal of Constructional Steel Research*. 2008;**64**(12):1463-1472. DOI: 10.1016/j.jcsr.2008.01.016
- [35] Popehn JRB, Schultz AE, Lu M, Stolarski HK, Ojard NC. Influence of transverse loading on the stability of slender unreinforced masonry walls. *Engineering Structures*. 2008;**30**(10):2830-2839. DOI: 10.1016/j.engstruct.2008.02.016
- [36] Buhan P, Felice G. A homogenization approach to the ultimate strength of brick masonry. *Journal of the Mechanics and Physics of Solids*. 1997;**45**(7):1085-1104. DOI: 10.1016/S0022-5096(97)00002-1
- [37] Milani G, Lourenco PB, Tralli A. Homogenised limit analysis of masonry walls, part I: Failure surfaces. *Computers & Structures*. 2006;**84**(3-4):166-180. DOI: 10.1016/j.compstruc.2005.09.005
- [38] Brasile S, Casciaro R, Formica G. Finite element formulation for nonlinear analysis of masonry walls. *Computers & Structures*. 2010;**88**(3-4):135-143. DOI: 10.1016/j.compstruc.2009.08.006

- [39] Köksal HO, Doran B, Turgay TA. Practical approach for modeling FRP wrapped concrete columns. *Construction and Building Materials*. 2009;**23**(3):1429-1437. DOI: 10.1016/j.conbuildmat.2008.07.008
- [40] Doran B, Köksal HO, Turgay T. Nonlinear finite element modeling of rectangular/square concrete columns confined with FRP. *Materials & Design*. 2009;**30**(8):3066-3075. DOI: 10.1016/j.matdes.2008.12.007
- [41] Mohamad G, Lourenco PB, Roman HR. Mechanical Behavior Assessment Of Concrete Block Masonry Prisms Under Compression. *International Conference on Concrete for Structures*. Coimbra, Portugal; 2005. p. 261-268
- [42] Kaushik HB, Rai DC, Jain SK. Stress-strain characteristics of clay brick masonry under uniaxial compression. *Journal of Materials in Civil Engineering*. 2007;**19**(9):728-739. DOI: 10.1061/(ASCE)0899-1561(2007)19:9(728)
- [43] Chen WF, Han DJ. *Plasticity for Structural Engineers*. New York: Springer-Verlag; 1988. p. 600
- [44] Maiolino S, Luong MP. Measuring discrepancies between coulomb and other geotechnical criteria: Drucker-Prager and Matsuoka-Nakai. 7th EUROMECH Solid Mechanics Conference. Lisbon, Portugal; 7-11 September 2009
- [45] Chen WF, Lui EM. *Structural Stability: Theory and Implementation*. New York: Elsevier; 1987. p. 486
- [46] Haach VG, Vasconcelos G, Lourenco PB. Influence of the geometry of units and filling of vertical joints in the compressive and tensile strength of masonry. *Special Issue of Materials Science Forum*. 2010;**636-637**:1321-1328. DOI: 10.4028/www.scientific.net/MSF.636-637.1321
- [47] Marcari G, Fabbrocino G, Manfredi G, Prota A. Experimental and numerical evaluation of tuff masonry panels shear seismic capacity. 10th North American Masonry Conference. St. Louis, USA; 2007
- [48] La Mendola L, Failla A, Cucchiara C, Accardi M. Debonding phenomena in CFRP strengthened Calcarene masonry walls and vaults. *Advances in Structural Engineering*. 2009;**12**(5):745-760. DOI: 10.1260/136943309789867872
- [49] Rahman A, Ueda T. In-plane shear performance of masonry walls after strengthening by two different FRPs. *Journal of Composites for Construction*. 2016;**20**(5):1-14. DOI: 10.1061/(ASCE)CC.1943-5614.0000661

